SERS-based monitoring of the intracellular pH in endothelial cells

Analyst

PAPER

View Article Online
View Journal | View Issue

Cite this: *Analyst*, 2015, **140**, 2321

SERS-based monitoring of the intracellular pH in endothelial cells: the influence of the extracellular environment and tumour necrosis factor-α†

Aleksandra Jaworska,[a,b] Lauren E. Jamieson,[c] Kamilla Malek,*[a,b] Colin J. Campbell,[c] Jaebum Choo,[d] Stefan Chlopicki[b,e] and Malgorzata Baranska[a,b]

Received 30th October 2014,
Accepted 20th November 2014

DOI: 10.1039/c4an01988a

www.rsc.org/analyst

The intracellular pH plays an important role in various cellular processes. In this work, we describe a method for monitoring of the intracellular pH in endothelial cells by using surface enhanced Raman spectroscopy (SERS) and 4-mercaptobenzoic acid (MBA) anchored to gold nanoparticles as pH-sensitive probes. Using the Raman microimaging technique, we analysed changes in intracellular pH induced by buffers with acid or alkaline pH, as well as in endothelial inflammation induced by tumour necrosis factor-α (TNFα). The targeted nanosensor enabled spatial pH measurements revealing distinct changes of the intracellular pH in endosomal compartments of the endothelium. Altogether, SERS-based analysis of intracellular pH proves to be a promising technique for a better understanding of intracellular pH regulation in various subcellular compartments.

Introduction

Intracellular pH (pH_i) regulation is critical for most cellular processes including cell volume regulation, vesicle trafficking, cellular metabolism, cell membrane polarity, muscular contraction, and cytoskeletal interactions.[1] In addition, some growth-stimulating signals including epidermal growth factor, platelet-derived growth factor, insulin, vasopressin, and serum activate the sodium–proton exchange activity to induce cellular alkalinisation and are thus important in cell activation, growth, and proliferation.[1] The endothelium, lining the interior of the whole circulation, which may be regarded as the largest functional organ in the human body, plays an active role in vasoregulation, coagulation, inflammation, and microvascular permeability.[2] In most if not all of these processes changes in the intracellular pH may be of importance. Indeed, it was demonstrated that endothelial alkalinisation inhibits gap junction communication and endothelium-derived hyperpolarisation.[3] In turn, a decrease in pH_i may result in the diminished production of nitric oxide.[4]

Tumour necrosis factor-α (TNFα) induces endothelial inflammation.[5] It inhibits the anticoagulatory mechanism and promotes thrombotic processes, which are responsible for venous thrombosis, arteriosclerosis, vasculitis, and disseminated intravasal coagulation.[5] Moreover, several chronic and acute human pathologies are associated with various degrees of endoplasmatic acidosis.[6] Failure of intracellular pH regulation may result in malfunction of various other enzymes and transduction pathways and may well contribute to various facets of the phenotype of endothelial dysfunction.[6]

There are only a few techniques that can be employed for the determination of pH_i such as pH-sensitive microelectrodes, nuclear magnetic resonance and fluorescence.[1] Until now, fluorescence spectroscopy has been shown to be the most sensitive and commonly used technique to measure pH_i.[1,7–9] In addition, pH-sensitive organic probes or fluorescent proteins can be functionalized to target specific cellular compartments, detecting pH from 4.7 (in lysosomes) to 8 in mitochondria.[7–10 and therein] However, low sensitivity, signal from background and photobleaching of fluorophores limit the application of fluorescence microscopy. An alternative technique is surface enhanced Raman spectroscopy. Briefly, nanoparticles (gold, silver, and carbon nanotubes *etc.*) are conjugated to pH-sensitive Raman reporters. The most commonly used compounds in the current approaches are 4-mercaptobenzoic acid,[11–17] 2-aminothiophenol[18] or 4-mercaptopyridine.[19] In an early application of SERS for measurements of pH_i, Talley *et al.*[11] have shown that the SERS signal from MBA adsorbed on silver nanoparticles is sensitive within 1 unit on the pH scale. The use of hollow gold nanoparticles as a SERS support improved the sensitivity to *ca.* 0.5 unit of pH as shown in SERS studies on pH_i in Chinese

[a]*Faculty of Chemistry, Jagiellonian University, 3 Ingardena Str., 30-060 Krakow, Poland. E-mail: malek@chemia.uj.edu.pl; Fax: +48-12634-0515; Tel: +48-12663-2064*
[b]*Jagiellonian Centre for Experimental Therapeutics (JCET), Jagiellonian University, 14 Bobrzynskiego Str., 30-348 Krakow, Poland*
[c]*EaStCHEM, School of Chemistry, University of Edinburgh, Edinburgh, EH9 3JJ, UK*
[d]*Department of Bionano Engineering, Hanyang University, Sa-1-dong 1271, Ansan 426-791, South Korea*
[e]*Department of Experimental Pharmacology, Jagiellonian University Medical College, Grzegorzecka 16, 31-531 Krakow, Poland*
†Electronic supplementary information (ESI) available. See DOI: 10.1039/c4an01988a

hamster ovary cells.[12] Scaffidi and co-workers[13] have applied pH-sensitive plasmonic-active fiber-optic nanoprobes to measure the intracellular pH in human mammary epithelial (HMEC-15/hTERT) and PC-3 human prostate cancer cells, showing that such *in situ* pH_i measurements correctly determine the intracellular acidity. The most innovative application of SERS for pH measurements has been reported by Cong and others[20] where the intracellular pH was measured using MBA-coated AuNPs embedded into silica nanopeapods *in vitro* and *in vivo*.

In our work, we evaluate the usefulness of SERS imaging with MBA-AuNP probes for monitoring pH_i dysregulation due to pH stress from the extracellular environment. In addition, we investigate the *in vitro* pH response in human umbilical vein endothelial cells (EA.hy926) upon their stimulation with tumour necrosis factor (TNFα).

Experimental

Materials

All compounds used in the fabrication of Au nanoparticles and preparation of buffers and 4-mercaptobenzoic acid (MBA) were purchased from Sigma-Aldrich and were of analytical grade. Deionized water (Millipore Milli-Q grade) with a resistivity of 18.2 MΩ was used in all the experiments. A solution of 4-mercaptobenzoic acid at a concentration of 1×10^{-3} M was prepared by diluting an appropriate mass of the solid in ethanol. Gold nanoparticles (AuNPs) with an average diameter of 40 nm were prepared according to the Frens procedure.[21] UV-Vis spectra, DLS (Dynamic Light Scattering) and AFM measurements confirmed the size of nanoparticles and excluded their aggregation due to interactions with MBA, similar to our previous work.[22] We applied 40 nm gold nanoparticles to EA.hy926 endothelial cells for which the uptake mechanism has been well-established in our previous studies.[22,23] For the collection of SERS spectra, 100 μL of 1×10^{-3} M solution of MBA was mixed with 1 mL of gold colloid. After 5 min vortexing, the mixture was centrifuged for 10 min at 3000 rpm and the supernatant was re-dissolved in DPBS (Dulbecco's phosphate-buffered saline). 0.1 M aqueous solutions of sodium hydroxide, sodium phosphate, disodium hydrogen phosphate, sodium dihydrogen phosphate and phosphate acid were used for preparing buffers in the pH range of 1–12.

To determine pH calibration curves, MBA-AuNP solution was mixed with a phosphate buffer of a given pH (5 : 1 v/v), then placed in a 96-well plate and SERS spectra were collected. The relative intensity of SERS bands assigned to the stretching modes of the carboxylate group and aromatic ring was calculated using OPUS 7.2 software by using unprocessed SERS spectra and plotted against pH. Finally, an equation was fitted to a calibration curve using Gnuplot software.

Cell culture

Experiments were conducted for EA.hy926 cells, a line derived from human umbilical vein endothelial cells fused with the A549 line. Cells were grown in plastic wells in DMEM supplemented with 10% fetal bovine serum, 2 mM L-glutamine, penicillin, streptomycin, and 2% HAT. Where cells were treated with TNFα, the medium was replaced with a medium containing 10 ng mL^{-1} TNFα and cells were incubated for 12 hours. Then, for all cells, the medium was replaced by a medium containing a solution of MBA-AuNPs. Briefly, the medium was mixed with the MBA-AuNP solution in the ratio of 10 : 1 (v/v). The final concentration of MBA-AuNPs in the medium was 1×10^{-11} M. Cells were incubated in the medium containing pH sensors for 0.5, 1, 2, 4 and 12 hours. Next, the cells were washed three times with DPBS to eliminate most of the residual nanoparticles left outside of the cell. In the next step, cells were stressed by incubation (10 min) in buffers with a pH of 3.93, 6.21, 7.20, 8.60 and 11.35. Then, SERS maps of live cells were immediately collected. For each buffer, SERS maps from 5 cells were collected, as under these conditions we could observe relatively fast progression in the loss of cell viability (up to 1 h). The total time of mapping of one cell was *ca.* 5 min, and only live and healthy cells were selected for the measurement, determined by their morphological characteristics such as shape and adhesion.

Instrumentation

Electronic absorption spectra of the gold colloid, 4-mercaptobenzoic acid and the gold colloid functionalised with MBA were recorded with a UV-Vis-NIR Perkin Elmer spectrophotometer (model Lambda 35) in the range of 200–1100 nm with a resolution of 2 nm using quartz cells of 1 cm path length. SERS mapping of cells and SERS spectra of MBA in buffers were recorded by using a WITec system, equipped with a He–Ne laser (632.8 nm). For all measurements, the integration time was 0.04 s with a single accumulation and laser power of 10 mW. The recorded spectral range for grating 600 g mm^{-1} was 0–2400 cm^{-1}. SERS spectra of MBA-AuNPs were recorded by placing a sample in a plastic 96-well plate and using an air objective (20×). Three SERS spectra were acquired, each for freshly prepared samples. For Raman mapping, raster scans over single living cells were carried out with a computer-controlled *x*,*y*-stage under an immersion objective with a magnification of 60×. The mapping step was 1 μm.

Analysis of SERS maps

Hierarchical K-means cluster analysis of SERS maps was performed using WITec Project 2.06 software. The spectra were analysed in the region of 200–1800 cm^{-1} after a routine procedure for cosmic ray removal and smoothing (13 points) using a Savitzky–Golay algorithm which improves the signal to noise ratio. A number of classes were chosen by the comparison of spectral profiles of their mean spectra. We started our analysis from 10–12 classes and then, if mean spectra were identical in the region of the marker bands, classes were merged. Cluster analysis was performed for each cell separately. pH_i values presented in the work were calculated from mean SERS spectra.

Results and discussion

pH calibration curves

Calibration curves were determined in the range of pH from 1 to 12. As discussed in detail previously,[11,24] the two SERS bands are sensitive to pH changes and this agrees with our SERS spectra of MBA shown in Fig. 1A. They are assigned to the symmetric stretching of the COO^- group [$\nu_s(COO)^-$] and the stretching vibration of the C═O bond in the COOH group at ~1420 and ~1720 cm^{-1}, respectively. Going toward acidic pH, the intensity of the 1720 cm^{-1} band increases, whereas the neutral and alkaline environments cause deprotonation of the COOH group resulting in an increase in the intensity of the $\nu_s(COO)^-$ mode along with its shifting from *ca.* 1400 to *ca.* 1420 cm^{-1}, *cf.* the inset in Fig. 1A. The strongest SERS bands at 1070 and 1580 cm^{-1}, attributed to the ν_{12} and ν_{8a} aromatic ring vibrations, respectively, are not sensitive to pH changes and were used for calculation of the relative intensities. We determined calibration curves representing the spectral changes as a function of pH by calculating heights as well as integral intensities of SERS bands at 1070, 1400–1420, 1580 and 1720 cm^{-1} individually for each raw spectrum. Fig. 1B illustrates exemplary calibration curves for the ratios $I_{1400-1420}/I_{1070}$ and I_{1720}/I_{1070}. They represent typical Henderson–Hasselbalch plots.[25] Several reports have shown similar calibration curves for the pH dependence of SERS signals of MBA but they usually estimate pH_i values by comparing calibration spectra with SERS spectra from cells.[11,13,15,17] Therefore, we additionally fitted an equation to the curves to give a simple mathematical formulation for the determination of pH based on spectral changes of 4-mercaptobenzoic acid, see Table 1. Slopes of both the plots in Fig. 1B show noticeable spectral changes in the pH range of 5–9 that corresponds to the natural pH range determined in the cellular compartments, *i.e.* from 4.7 in lysosomes to 8 in mitochondria.[26] The error calculated for eqn (1) was ±0.15 of pH value. For comparison, the error of pH measurements by using fluorescence labels is *ca.* ±0.3 according to Wu and co-workers.[27]

In vitro SERS-based pH_i imaging

In our previous study on the cellular uptake of R6G-AuNPs by EA.hy926 cells (R6G – rhodamine 6G), we observed the SERS signal of the Raman reporter just after 0.5 h of incubation and then saturation of the nanoparticles appeared after 2 h incubation.[23] A longer incubation time of more than 2 hours resulted in a slow process of de-attaching molecules of the dye from the gold surface. Since the MBA molecules interact with the

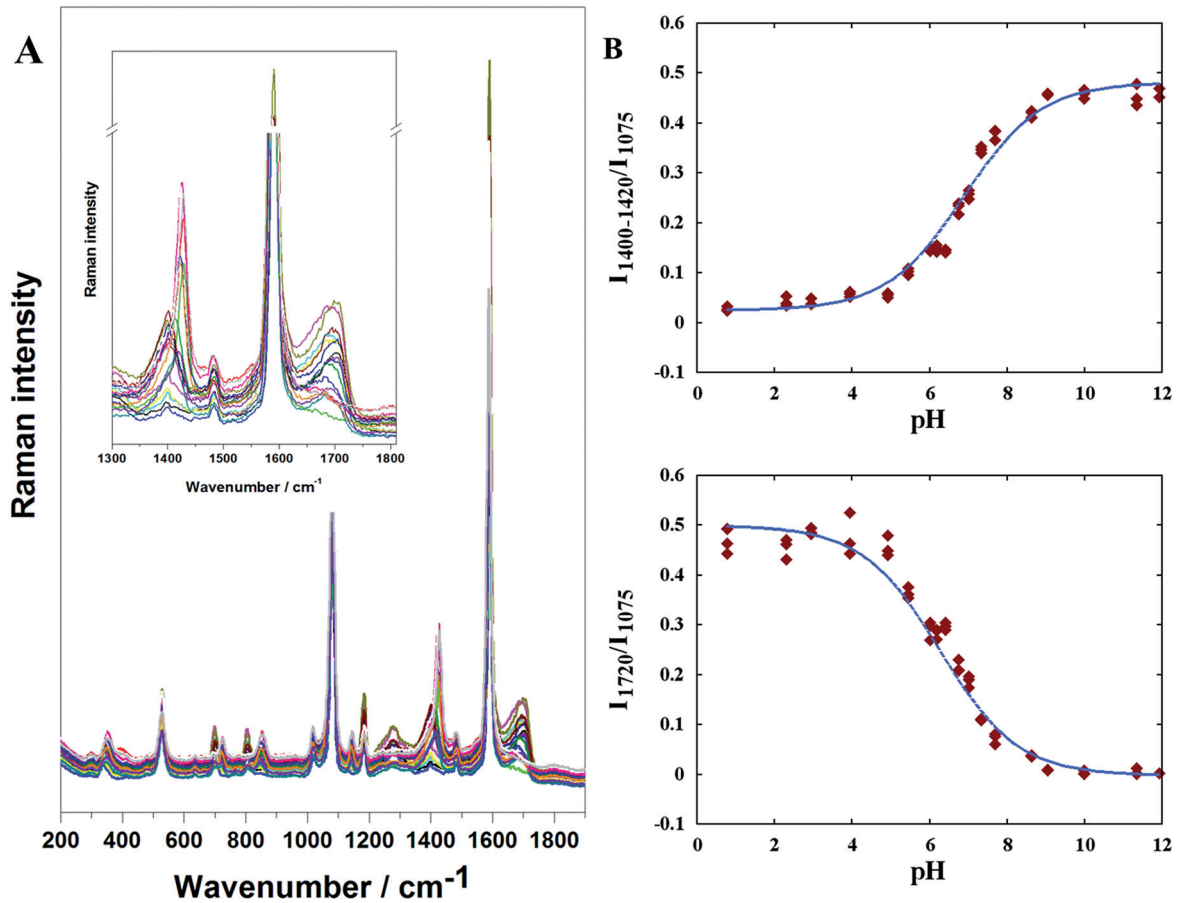

Fig. 1 (A) SERS spectra of MBA at different pH values from 1 to 12. The inset shows the region of 1300–1800 cm^{-1} associated with pH-sensitive bands at *ca.* 1400–1420 and 1720 cm^{-1}; (B) Henderson–Hasselbalch plots for band ratios: $I_{1400-1420}/I_{1070}$ (top) and I_{1720}/I_{1070} (bottom).

metal surface in a different way than rhodamine 6G, we optimized the incubation time for MBA-AuNPs to examine saturation of cells by nanoprobes and to avoid incubation resulting in their substitution by cellular biomolecules. Fig. 2 displays SERS maps showing the intensity of the 1070 cm^{-1} band in endothelial cells incubated with MBA-AuNPs for 0.5–12 hours and SERS spectra randomly chosen from these maps. They illustrate that the overall intensity of the SERS signal increases upon elongation of incubation time and the largest number of nanosensors entered the intercellular space after overnight incubation. Kneipp and co-workers have shown that MBA-AuNPs are distributed all over the cytosol in mouse fibroblast cells after 4.5 h and a longer incubation time does not change the distribution of nanosensors[14] while the 6 h and 12 h incubation were applied in experiments with mouse macrophage and Chinese hamster ovary cells, respectively.[11,15] This indicates that the optimal incubation time should be determined for each cell type as it may considerably differ.

No SERS bands originating from cellular biocomponents were found in spectra indicating the stability of interactions between MBA and the gold while SERS marker bands for pH were not observed before the 4 h incubation however, they exhibited a low signal to noise ratio. Therefore, the 12 h incubation was applied in the further experiments. Moreover, apart from typical SERS features of 4-mercaptobenzoic acid observed in spectra displayed in Fig. 1A, we found the presence of anomalous bands in SERS spectra at ~1000 and ~1025 cm^{-1}, *cf.* Fig. 2. The other reports regarding the application of MBA for determination of pH_i have also shown the presence of these bands when the sensor molecules were anchored to AgIF fiber-optic nanoprobes,[13] hollow gold nanospheres,[12] silver nanoparticles[11] whereas they were absent when MBA-AgNPs were encapsulated in silica[15] and when MBA-AgNPs in cells were probed using surface enhanced hyper-Raman scattering (SEHRS).[28] This indicates that the appearance of these bands does not depend on the properties of the metal surface. Michota and Bukowska have shown in their studies on the adsorption process of MBA on silver and gold roughened electrodes that the 1000 and ~1025 cm^{-1} bands are typical for monosubstituted benzene derivatives and their presence in SERS spectra of MBA may result from the decarboxylation process of these molecules.[24] This process can be additionally accelerated in an alkaline environment and appears even after 20 minutes after adsorption. Since our calibration spectra do not show the

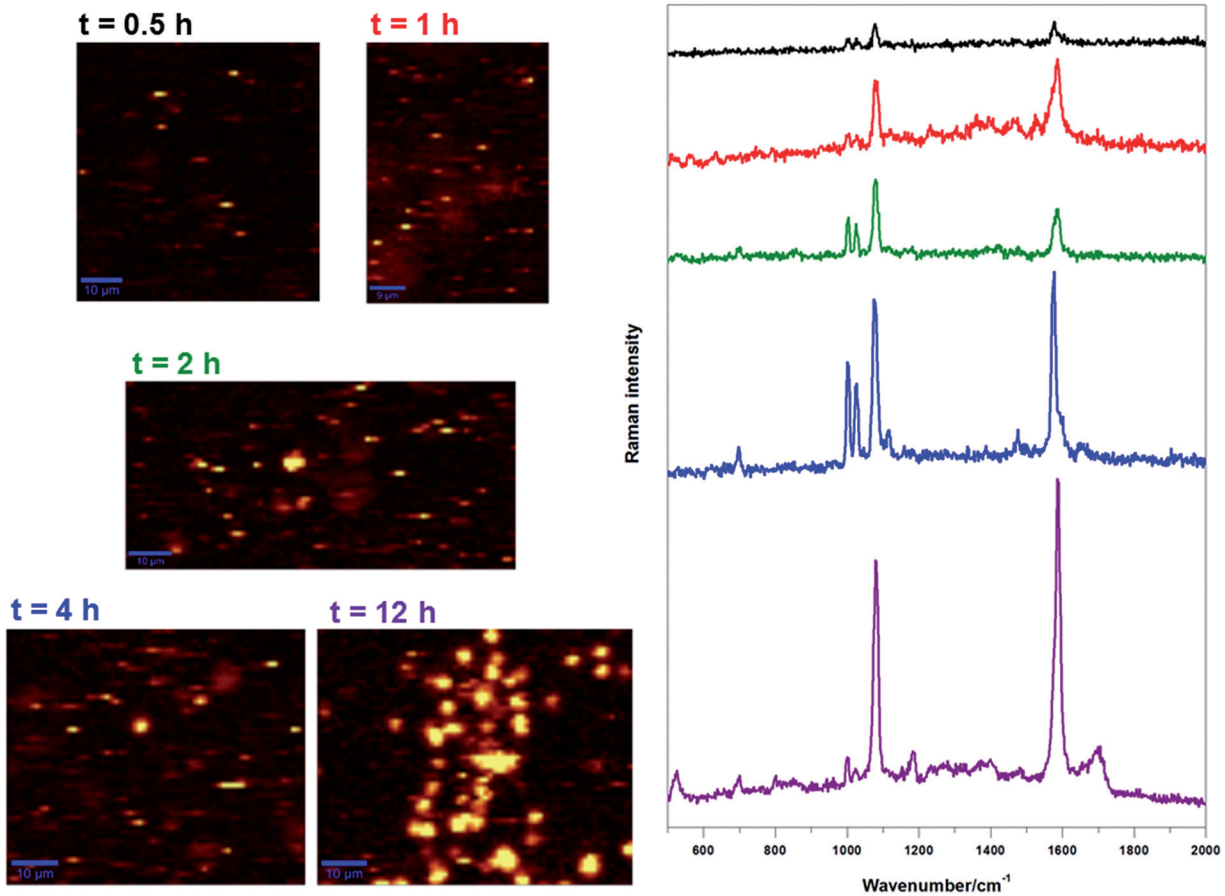

Fig. 2 SERS maps constructed by integration of the 1070 cm^{-1} band for EA.hy926 cells incubated in medium (pH = 7.20) containing MBA-AuNPs for 0.5, 1, 2, 4 and 12 h. The same intensity scale is applied for each map. SERS spectra of MBA (right) were extracted from pixels of the maps representing the highest intensity of the 1070 cm^{-1} band. Colours of spectra correspond to the incubation time of 0.5 (black), 1 (red), 2 (green), 4 (blue) and 12 h (purple). Microphotographs of cells for the SERS maps are displayed in Fig. S2 (in the ESI†).

presence of these bands while some SERS spectra of cells do, we speculate that decarboxylation of MBA molecules anchored to AuNPs can result from the microenvironment process, *e.g.* interactions of nanosensors with other molecules through the MBA carboxylate group.

Next, we investigated the effects of extracellular pH changes on SERS nanosensors and consequently on the intracellular pH in endothelial cells. The incorporation of MBA-AuNPs did not bring a significant change to the cell morphology and no obvious cell death was found. This is not surprising since similar nanosensors have been shown to be non-toxic using biochemical assays.[22,29–31] Fig. 3 shows the presence of the targeted nanosensors in EA.hy926 cells incubated in the buffers with pH 3.9, 6.2, 8.6 and 11.3. The control cells were incubated only in DPBS (pH: 7.2), see Fig. 3C. To simplify our analysis, we performed K-means cluster analysis and a number of classes were chosen based on spectral differences in the pH-sensitive spectral region. Then pH values were calculated for the mean spectra from cluster analysis according to eqn (1) in Table 1.

For control cells, we observed changes in pH_i from 6.5 to 9.8. Pixels decoding pH values are unevenly distributed within the intercellular space of the endothelial cells, *cf.* Fig. 3C. The observed range of pH indicates that the 12 h uptake of the nanosensors results in a marked lack of delivery to low pH (4.7–6.3) compartments like early stage endosomes and lysosomes. The red and blue classes, pH values of 6.5 and 6.8, respectively, can correspond to recycling of endosomes.[26,32] In turn, the green and grey classes for which pH values vary from 7.2 to 7.6 exhibit the environment of cytosol. Although the current studies on the internalisation of particles through formation and maturation of the endocytic system do not predict a direct release of nanoparticles from vesicles to the cytosol, except a specific process of backfusion, in which lysosomal degradation can appear,[33] TEM and fluorescence studies on intracellular trafficking of various nanoparticles have implicated their presence in the cytosol, mitochondria and Golgi apparatus.[34–36] This may be associated with saturation of the endosomal–lysosomal compartments by nanoparticles and their leakage to the cytosol. The cluster analysis also differentiated a cellular area with pH in the range of 8.8–9.8, the black and purple classes. This unusual H^+/OH^- balance for the healthy cells can result from variation in the adsorption process and/or decomposition of 4-mercaptobenzoic acid on the gold surface hence we observed intensification of the anomalous bands in mean SERS spectra corresponding to these pH values, *cf.* Fig. S2C (in the ESI†).

Stimulating extreme stress conditions for cells by keeping them in a relatively acidic (pH: *ca.* 4) or alkaline environment (pH: *ca.* 11) resulted in inducing appropriate changes in pH_i in a very narrow range of values in comparison to other experimental conditions applied in our work, *cf.* Fig. 3A and E. Reducing the extracellular pH from 7.2 typical for the medium solution to 3.9 led to a high uptake of the pH sensors and decreasing the pH_i of cytoplasm to 5.4 (pink class in Fig. 3A). This remarkable accumulation of nanosensors can be associated with increased acidification of early and recycling endosomes that shifts the balance from recycling endosomes to the lysosome formation as shown previously by the effects of inhibition of the Na^+/H^+ exchanger by amiloride in the RBL-2H3 mast cell line.[32] The blue class surrounding the pink area and located close to the cellular membrane indicates an increase of pH to 6.3. It is well-known that nanoparticles enter the intercellular space through the process of endocytosis and that accumulated endosomes are converted into lysosomes. Thus, the observed pH of 6.3 likely corresponds to early sorting of endosomes which then accumulate in the cytosol of the cell in the form of late endosomes that in turn exhibit an average pH of 5.4.[26,37,38] Interestingly, a range of pH typical for the endosomes–lysosome conversion (4.7–6.5) was not found when the endothelial cells were exposed to the highly alkaline environment (Fig. 3E). The concentration of the nanoparticles functionalised with MBA is much lower in this case than for the acidic conditions of cell culture. The MBA-AuNPs are distributed along the cellular membranes of the three endothelial cells in cellular compartments with pH 8.4 with a small contribution of pH 8.5. The cluster analysis discriminated also the blue class for a SERS spectrum exhibiting the spectral profile of the decarboxylated MBA molecules.[24] According to the literature,[26] pH of *ca.* 8 is likely to be found in mitochondria however, we do not expect that the SERS imaging reports directly on these cellular compartments. It seems more likely that the endosomal–lysosomal system responds to increasing pH through inhibition of the H^+ ATPase pump as shown in numerous reports.[26,32,39,40] The other reason could be an increase in cytosolic pH due to the alkaline buffer, affecting the overall H^+/OH^- equilibrium in all cellular compartments. We also investigated a mild effect of the extracellular environment on the regulation of pH_i. For this purpose, the endothelial cells were exposed to buffer solutions with pH different from the typical culture conditions by 1 unit, see Fig. 3B and D. The range of pH for the cells incubated in the buffer with pH 6.2 is 6.9–8.1 and the concentration of the nanoprobes in a cell is relatively low in comparison to strongly acidic and physiological conditions, *cf.* Fig. 3A and C. The qualitative assessment of the distribution of pH_i in the cluster map shown in Fig. 3B indicates that the highest pH, 7.6 and 8.1, is spatially localised within a few pixels of the SERS image of the cells. This observation suggests that exposing endothelial cells to a mildly acidic environment does not strongly affect the cellular processes of endocytosis or the SERS technique is not sensitive enough to determine such a cellular response. The latter is more possible, as pH 7.0 inhibits chemically induced apoptosis in a specific endothelial cell line, suggesting that the effects of altered extracellular pH may be cell type dependent.[41] On the other hand, our results agree well with fluorescence spectroscopy studies on endothelial cells from rat aorta.[7] In contrast, increasing the extracellular pH to 8.6 discriminates pH_i from 5.8 to 9.1 related mainly to early and late endosomes (pH: 5.8–6.8). An increase of pH_i to 7.5 and 9.1 correlates well with a high intensity of a SNARF-1 fluorophore used in confocal fluorescence measurements of the endothelial layer in the animal aorta cross-sections.[7] In this report, extracellular alkalinisation to pH 8.6 was also associated with an increase of the NO concentration which serves as a specific biochemical marker for the

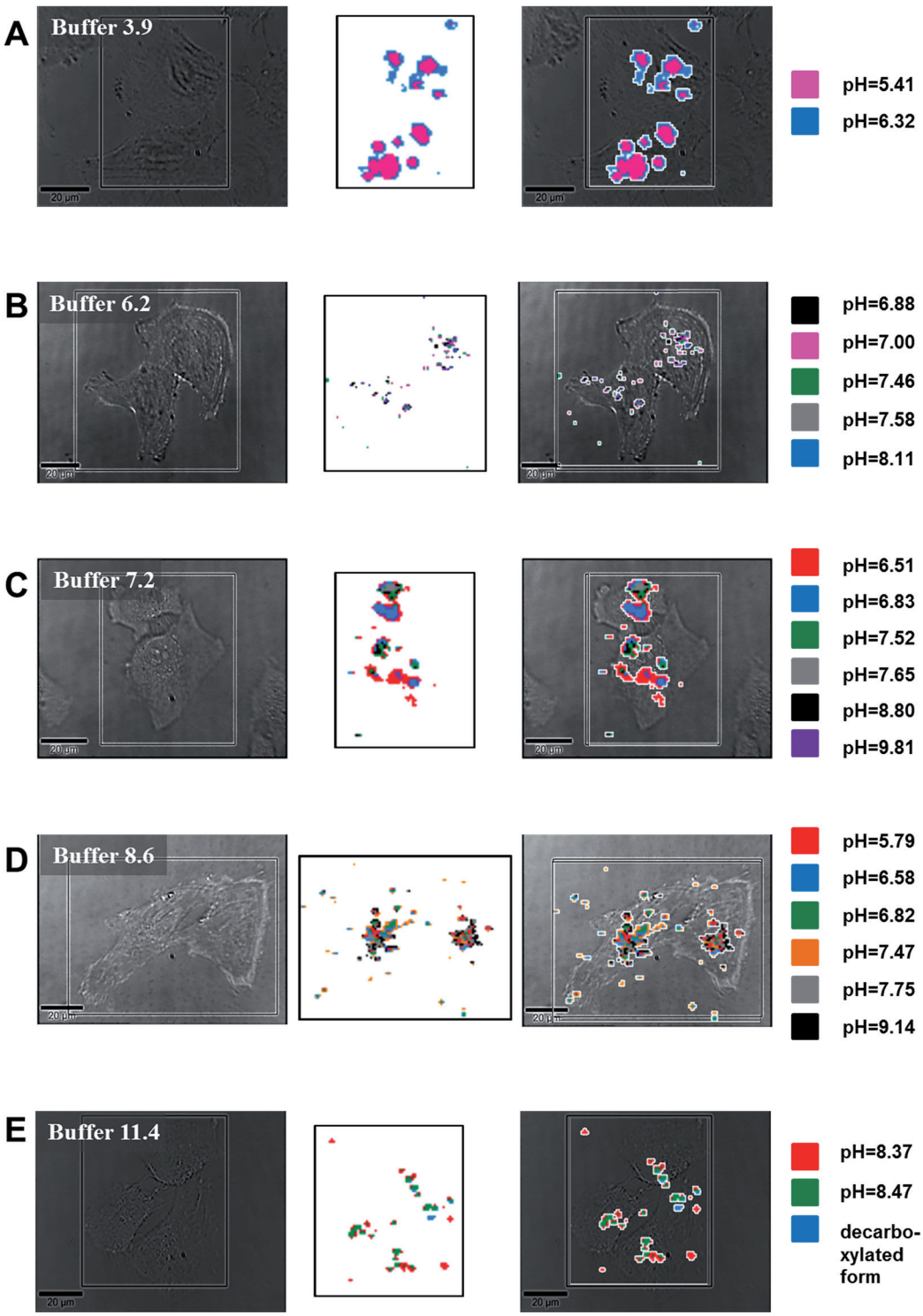

Fig. 3 Microphotographs and cluster maps of SERS-based pHi imaging for EA.hy926 cells incubated with MBA-AuNPs in buffers with pH 3.9 (A), 6.2 (B), 7.2 (C), 8.6 (D) and 11.4 (E). The colours decoded in the cluster maps correspond to pH values labelled by squares.

endothelial dysfunction.[42] Endothelial inflammation may be induced by tumour necrosis factor-α.[5,42] Fig. 4 displays the distribution of pH-sensitive nanosensors in TNFα incubated endothelial cells. First of all, the cluster maps show a high accumulation of the functionalised gold nanoparticles in the impaired endothelial cells similar to those found for cells exposed to the highly acidic extracellular environment (see Fig. 3A) and to cancerous cells.[43] Oku *et al.* showed that under certain conditions TNFα may increase the membrane permeability,[44] which can explain the relatively pronounced uptake

Table 1 The Henderson–Hasselbalch equation determined from calibration curves shown in Fig. 1B along with calculated coefficients[a] and their root mean square error (RMSE, in %)

r	$I_{1400-1420}/I_{1070}$	RMSE	I_{1720}/I_{1070}	RMSE
$\mathrm{pH} = d + \ln\frac{r-a}{b-r}$ (1)				
a	0.024	2.26	0.499	0.76
b	0.481	0.53	0.0027	65.0
d	6.876	2.00	6.273	2.65

[a] r – relative intensity of the selected bands; a, b and d – equation coefficients.

of nanoparticles to the TNFα-treated cells. It was shown that TNFα induced mitochondrial membrane depolarisation, increased intracellular Ca^{2+} concentration, released cytochrome c resulting in disruption of cytosolic pH.[45,46] Fig. 4 shows TNFα treated cells that display the characteristic rounding and blebbing. The cluster analysis shows a more uniform distribution of nanosensors throughout the cytosol – this suggests a disruption of the endocytic pathway leading to nanosensor release into the cytosol or high increase in formation of endosomes in TNFα – activated cells. Cluster maps in Fig. 4 show that the pH_i varies from 5.5 to 7.2. This reflects endocytic recycling pathways.[47] In Fig. 4A, we observe a conversion between late endosomes (red class, pH 5.5) and endocytic recycling compartments[47] or early endosomes[19] (blue class, pH 6.4) localized along the cellular membrane. Next, the response for the TNFα-induced intracellular imbalance may also result in lowering of cytosol pH, observed in the beige class (pH 7.1). A slightly different picture is illustrated in Fig. 4B, for which we do not observe pH typical for late endosomes.

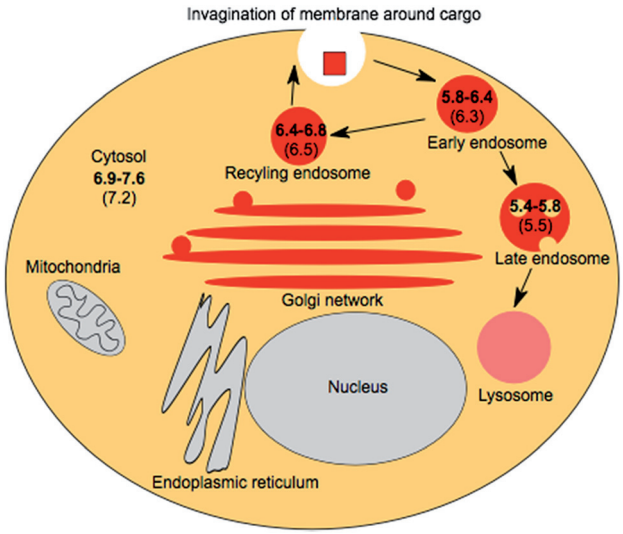

Fig. 5 A scheme of cell regions and pH determined in this work (in bold) along with the pH of cell compartments from ref. 26 (in brackets).

Conclusions

These experiments demonstrated that using targeted gold nanoparticles functionalized with 4-mercaptobenzoic acid allowed the detection of changes in pH_i induced by short-term alkalization or acidification of the extracellular environment of endothelium. Using SERS-based pH_i mapping, we also demonstrated that the TNFα-induced response in the endothelium was associated with intracellular acidosis. In all experiments, we were able to follow the endocytic pathway in cells, as calcu-

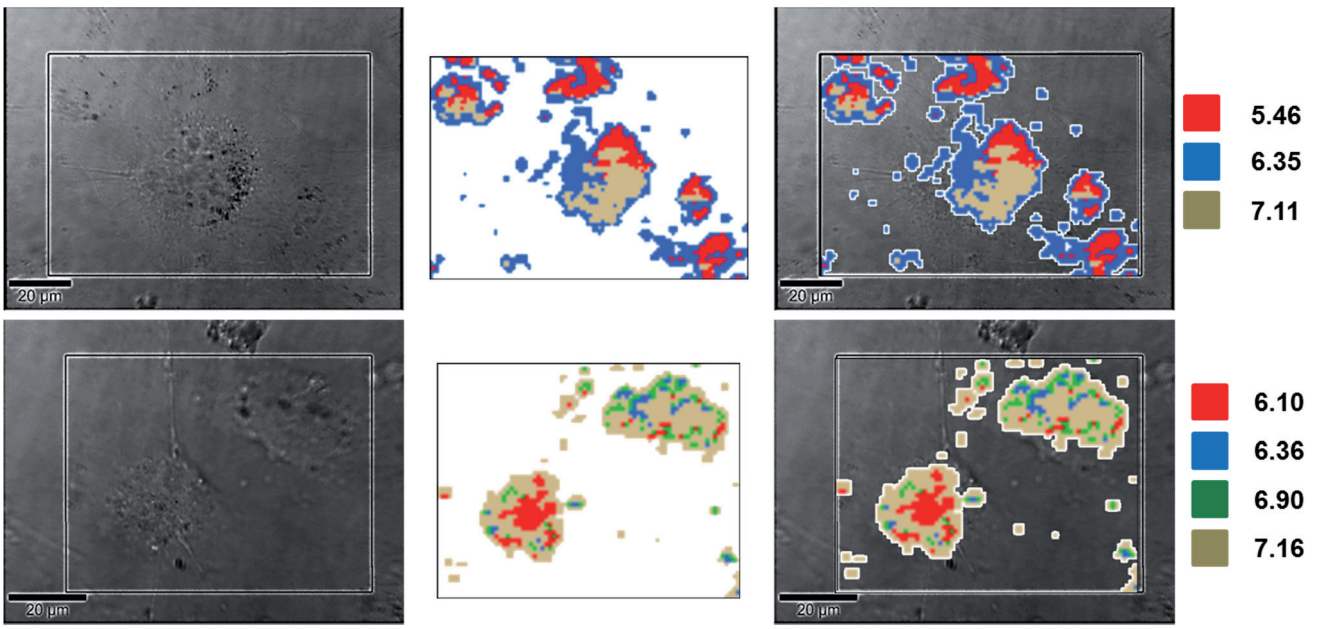

Fig. 4 Microphotographs and cluster maps of SERS-based pHi imaging for TNFα-incubated EA.hy926 cells. The colours decoded in the cluster maps correspond to pH values labelled by squares. SERS maps of control cells for this experiment are shown in Fig. 3C.

lated pH values were correlated with the pH of endosomes at different stages of maturation. We summarised our findings in Fig. 5. Moreover, we observed the differences between MBA-AuNPs' uptake by healthy and inflamed cells, which suggested TNFα-induced activation of uptake. In contrast to the determination of pH by fluorescence spectroscopy,[1] the MBA-AuNPs' uptake appears through endocytosis, which makes SERS a valuable tool to study different stages of this process. Altogether, SERS spectra of MBA exhibit a spectral signature suited for differentiation of pH_i values between 5 and 9, enabling probing of a variety of subcellular compartments and their response to environmental and pathological stimuli.

Acknowledgements

This work was supported by the National Center of Science (grant PRELUDIUM DEC-2012/05/N/ST4/00218) and by the European Union from the resources of the European Regional Development Fund under the Innovative Economy Programme (grant coordinated by JCET-UJ, no. POIG.01.01.02-00-069/09). We also thank the University of Edinburgh School of Chemistry for the Neil Campbell Travel Award for supporting LJ. We also thank Joanna Jałmużna from the Department of Mathematics and Computer Sciences, Jagiellonian University in Krakow for fitting the calibration curve using Gnuplot software.

References

1 F. B. Loiselle and J. R. Casey, in *Membrane Transporters in Drug Discovery and Development, Methods in Molecular Biology*, ed. Q. Yan, Springer Science + Business Media, LLC, 2010, vol. 637.
2 P. F. Davies, *Physiol. Rev.*, 1995, **75**(3), 519.
3 E. Boedtkjer, S. Kim and C. Aalkjaer, *J. Physiol.*, 2013, **591**(6), 1447.
4 E. Schulz and T. Münzel, *Circulation*, 2011, **124**, 1806.
5 K. Chatzantoni and A. Mouzaki, *Curr. Top. Med. Chem.*, 2006, **6**, 1707.
6 E. Crimi, F. S. Taccone, T. Infante, S. Scolletta, V. Crudele and C. Napoli, *J. Crit. Care*, 2012, **27**, 108.
7 V. K. Capellini, C. B. A. Restini, L. M. Bendhack, P. R. B. Evora and A. C. Celotto, *PLoS One*, 2013, **8**(5), e62887.
8 J. Zhou, C. Fang, T. Chang, X. Liu and D. Shangguan, *J. Mater. Chem. B*, 2013, **1**, 661.
9 P. Li, H. Xiao, Y. Cheng, W. Zhang, F. Huang, W. Zhang, H. Wang and B. Tang, *Chem. Commun.*, 2014, **50**, 7184.
10 K. Galler, K. Brautigam, C. Große, J. Popp and U. Neugebauer, *Analyst*, 2014, **139**, 1237.
11 C. E. Talley, L. Jusinski, C. W. Hollars, S. M. Lane and T. Huser, *Anal. Chem.*, 2004, **76**, 7064.
12 A. M. Schwartzberg, T. Y. Oshiro, J. Z. Zhang, T. Huser and C. E. Talley, *Anal. Chem.*, 2006, **78**, 4732.
13 J. P. Scaffidi, M. K. Gregas, V. Seewaldt and T. Vo-Dinh, *Anal. Bioanal. Chem.*, 2009, **393**, 1135.
14 J. Kneipp, H. Kneipp, B. Wittig and K. Kneipp, *J. Phys. Chem. C*, 2010, **114**, 7421.
15 F. Wang, R. Widejko, Z. Yang, K. T. Nguyen, H. Chen, L. P. Fernando, K. A. Christensen and J. N. Anker, *Anal. Chem.*, 2012, **84**, 8013.
16 S. W. Bishnoi, C. J. Rozell, C. S. Levni, M. K. Gheith, B. R. Johnson, D. H. Johnson and N. J. Halas, *Nano Lett.*, 2006, **6**(8), 1687.
17 S. Balint, S. Rao, M. Maroo, P. Miskovsky and D. Petrov, *J. Raman Spectrosc.*, 2011, **42**, 1215.
18 Z. Wang, A. Bonoiu, M. Samoc, Y. Cui and P. N. Prasad, *Biosens. Bioelectron.*, 2008, **23**, 886.
19 K. L. Nowak-Lovato and K. D. Rector, *Appl. Spectrosc.*, 2009, **63**(4), 387.
20 V. T. Cong, E. O. Ganbold, J. K. Saha, J. Jang, J. Min, J. Choo, S. Kim, N. W. Song, S. J. Son, S. B. Lee and S. W. Joo, *J. Am. Chem. Soc.*, 2014, **136**, 3833.
21 G. Frens, *Nature Phys. Sci.*, 1973, **241**, 20.
22 A. Jaworska, T. Wojcik, K. Malek, U. Kwolek, M. Kepczynski, A. A. Ansary, S. Chlopicki and M. Baranska, *Microchim. Acta*, 2014, DOI: 10.1007/s00604-014-1307-5.
23 A. Jaworska, K. Malek, N. Kachamakova-Trojanowska, S. Chlopicki and M. Baranska, *Biomed. Spectrosc. Imaging*, 2013, **2**, 183.
24 A. Michota and J. Bukowska, *J. Raman Spectrosc.*, 2003, **34**, 21.
25 N. Radić and A. Prkić, *Rev. Anal. Chem.*, 2012, **31**, 93.
26 J. R. Casey, S. Grinstein and J. Orlowski, *Nat. Rev. Mol. Cell Biol.*, 2010, **11**, 50.
27 M. M. Wu, J. Llopis, S. Adams, J. M. McCaffery, M. S. Kuloma, T. E. Machen, H. H. Moore and R. Y. Tsien, *Chem. Biol.*, 2000, **7**, 197.
28 J. Kneipp, H. Kneipp, B. Wittig and K. Kneipp, *Nano Lett.*, 2007, **7**(9), 2819.
29 C. A. R. Auchinvole, P. Richardson, C. McGuinnes, V. Mallikarjun, K. Donaldson, H. McNab and C. J. Campbell, *ACS Nano*, 2012, **6**, 888–896.
30 J. Jiang, C. Auchinvole, K. Fisher and C. J. Campbell, *Nanoscale*, 2014, **6**, 12104–12110.
31 M. A. Ochsenku, P. R. T. Jess, H. Stoquert, K. Dholakia and C. J. Campbell, *ACS Nano*, 2009, **3**, 3613–3621.
32 K. L. Nowak-Lovato, B. S. Wilson and K. D. Rector, *Anal. Bioanal. Chem.*, 2010, **398**, 2019.
33 J. Huotari and A. Helenius, *EMBO J.*, 2011, **30**, 3481.
34 M. Ekkapongpisit, A. Giova, C. Follo, G. Caputo and C. Isidoro, *Int. J. Nanomed.*, 2012, **7**, 4147.
35 J. Huang, C. Zong, H. Shen, M. Liu, B. Chen, B. Ren and Z. Zhang, *Small*, 2012, **8**, 2577.
36 R. R. Sathuluri, H. Yoshikawa, E. Shimizu, M. Saito and E. Tamiya, *PLoS One*, 2011, **6**, e22802.
37 S. H. Hansen, K. Sandvig and B. Van Deurs, *J. Cell Biol.*, 1991, **113**, 731.
38 S. Mukherjee, R. N. Ghosh and F. R. Maxfield, *Physiol. Rev.*, 1997, **77**, 759.

39 M. Bradley, L. Alexander, K. Duncan, M. Chennaoui, A. C. Jones and R. M. Sanchez-Martin, *Bioorg. Med. Chem. Lett.*, 2008, **18**, 310.
40 J. Liu, W. Lu, D. Reigada, J. nquyen, A. M. Laties and C. H. Mitchell, *Invest. Ophthalmol. Visual Sci.*, 2008, **49**(2), 772.
41 C. Terminella, K. Tollefson, J. Kroczynski, J. Pelli and M. Cutaia, *Am. J. Physiol.: Lung Cell. Mol. Physiol.*, 2002, **283**, L1291.
42 J. de Haro Miralles, E. Martınez-Aguilar, A. Florez, C. Varela, S. Bleda and F. Acin, *Interact. Cardiovasc. Thorac. Surg.*, 2009, **9**, 107.
43 S. Jung, J. Nam, S. Hwang, J. Park, J. Hur, K. Im, N. Park and S. Kim, *Anal. Chem.*, 2013, **85**, 7674.
44 N. Oku, R. Araki, H. Araki, S. Shibamoto, F. Ito, T. Nishihara and M. Tsujimoto, *J. Biochem.*, 1987, **102**(5), 1303.
45 Z. Jin, L. Pei and D. Wang, *Zhonghua Fuchanke Zazhi*, 2000, **35**, 657.
46 J. Cheng, W. Tang, Z. Su, J. Guo, L. Tong and Q. Wei, *Cancer Lett.*, 2012, **321**(2), 169.
47 F. R. Maxfield and T. E. McGraw, *Nat. Rev. Mol. Cell Biol.*, 2004, **5**, 121.